Measurement 257 (2026) 118660

Contents lists available at ScienceDirect

Measurement

journal homepage: www.elsevier.com/locate/measurement

A reconfigurable array and MIMO antenna for 18 GHz and 28/38 GHz applications

Halil Paşalıoğlu [a], Lulu Wang [d,e], Mehmet Bakır [f], Liton Chandra Paul [b], Erkan Tetik [c,1,*], Muharrem Karaaslan [a]

[a] Iskenderun Technical University, Department of Electrical and Electronics Engineering, Iskenderun, Hatay 31200, Türkiye
[b] Pabna University of Science and Technology, Electrical, Electronic and Communication Engineering, Pabna 6600, Bangladesh
[c] Usak University, Department of Instructional Technologies, Faculty of Education, Usak 6400, Türkiye
[d] Department of Engineering, Reykjavik University, Reykjavik, 102, Iceland
[e] College of Science, Engineering and Technology, University of South Africa, Midrand, 1686, Gauteng, South Africa
[f] Yozgat Bozok University, Faculty of Engineering-Architecture, Computer Engineering, Yozgat, 66100, Türkiye

ARTICLE INFO

Keywords:
Wireless communication
MIMO
Antenna arrays
5G communication

ABSTRACT

This study introduces the development and experimental verification of a reconfigurable array and MIMO antenna system designed to operate at 18 GHz, 28 GHz, and 38 GHz—frequency bands that are critically important for next-generation wireless communication technologies, including 5G and beyond. The reconfigurability of both antenna types is achieved through the integration and dynamic control of PINs, allowing for the selective activation and deactivation of specific segments defined by designated geometric parameters. Simulation and experimental results of the proposed antennas, including scattering parameters and radiation patterns, are thoroughly investigated. Simulation results indicate that the array antenna achieves bandwidths of 0.80 GHz at 18 GHz, 2.62 GHz at 28 GHz, and 7.91 GHz at 38 GHz, respectively. This performance encompasses all FCC-designated millimeter-wave 5G bands. The MIMO antenna demonstrates a transmission coefficient below −25 dB for both PIN diode states, significantly exceeding the −10 dB isolation threshold. This result confirms the antenna's suitability for operation across the 18 GHz, 28 GHz, and 38 GHz frequency bands. Subsequently, the fabrication of both antennas was undertaken, and the measured parameters exhibited good agreement with the simulation results. The reconfigurable array antenna exhibits beam steering and pattern diversity capabilities essential for overcoming propagation challenges at millimeter-wave frequencies, while the MIMO antenna system leverages spatial multiplexing and diversity to enhance data rates and link reliability. The presented antenna designs offer versatility for future wireless systems and hold considerable promise for a multitude of advanced applications, including high-capacity data transmission and radar systems operating within the 5G bands.

1. Introduction

The increasing demands of wireless and mobile communication necessitate higher bandwidths and data rates. Fifth generation (5G) communication technologies have been deployed to address this need, while research on sixth generation (6G) systems is underway. The adoption of 5G has led to a substantial increase in wireless information technology users and researchers [1,2]. 5G applications can utilize the 30–300 GHz millimeter-wave (mmWave) spectrum to achieve higher data rates [3,4]. Frequencies such as 25 GHz, 38 GHz, 60 GHz, and 73 GHz, allocated by the International Telecommunication Union, are commonly employed for high-speed, short-range communication [5,6]. Antenna design and fabrication at these frequencies present numerous challenges, most notably achieving sufficient bandwidth and miniaturization [7]. Multiple-input multiple-output (MIMO) systems, employing multiple antenna elements, offer a solution to these challenges [8,9]. MIMO technology has become prevalent in wireless communication due to its significant capacity enhancement capabilities [10]. As a crucial component of communication systems, antenna technology requires continuous development to meet the evolving demands of 5G and

* Corresponding author.
E-mail addresses: halilpasalioglu@yahoo.com (H. Paşalıoğlu), luluw@ru.is (L. Wang), mehmet.bakir@bozok.edu.tr (M. Bakır), litonpaulete@gmail.com (L.C. Paul), erkantetik@usak.edu.tr (E. Tetik), muharrem.karaaslan@iste.edu.tr (M. Karaaslan).
[1] ORCID: 0000-0002-8183-8141.

https://doi.org/10.1016/j.measurement.2025.118660
Received 9 May 2025; Received in revised form 3 August 2025; Accepted 5 August 2025
Available online 6 August 2025

beyond [11]. The 28 GHz/38 GHz band has garnered significant attention for 5G devices. Standard MIMO antenna configurations, typically comprising two or more elements, can fulfill these requirements.

Numerous studies have investigated MIMO antennas operating across various frequency ranges. For instance, [12] presents a MIMO antenna pair consisting of open-ended circular-ring slot radiators fed by independent semi-arc-shaped microstrip lines, exhibiting polarization diversity. Design of an enhanced Yagi-Uda antenna is introduced for dual-band operation at 28/38 GHz which is produced by a corrugated dipole strip and a capacitively end-coupled extension strip as the driving element in [13]. These types of antennas can be used for many different purposes in terms of design and operating range. Wen et al. [14] introduce a MIMO antenna design for metal-frame smartwatches, operating in the 2.4–2.49 GHz Bluetooth/Wi-Fi band. Khalid et al. [15] proposes a T-junction power combiner/splitter MIMO antenna for 5G applications, covering the 25.5–29.6 GHz range. Similarly, Sehrai et al. [16] present an H-shaped MIMO antenna design for 5G operation in the 36.83–40.0 GHz band. Cheng et al. propose an M × N molecular MIMO communication system with symmetric and asymmetric topologies [17]. A deep neural networks and Transformer-based model are proposed to predict the channel parameters in the channel impulse response of this molecular MIMO system. Mahmoud et al. [18] introduce a multi-polarized mmWave base station antenna for 5G, employing a 32-element array in an upside conical frustum configuration to achieve multi-beam patterns with directivity and polarization control. An electronic band gap (EBG) structure for a 28 GHz/38 GHz dual-band MIMO antenna, designed to improve radiation efficiency, is proposed in [19]. In [20], a 4-port dual-band printed MIMO antenna array operating at 28 GHz and 38 GHz in the mm-wave band for 5G communications is proposed. The suggested MIMO configuration offers a high gain of about 7.9 dB and 13.7 dB at 28 GHz and 37.3 GHz, respectively. Multi-element array technology for 5G applications, operating at 27 GHz and 39 GHz and offering maximum gains of 5 dBi and 5.7 dBi, respectively, is described in [21]. Ahmad et al. present a simple, miniaturized, and low-profile MIMO antenna operating at 29 GHz with reduced mutual coupling between the antenna elements for 5G communication [22]. A miniaturized dual-band MIMO antenna with wide bandwidth and high isolation using metamaterial structures is introduced by Khan et al. [23]. Yue et al. present the hybrid-field multipath channel estimation in holographic MIMO communications [24]. MIMO and array antenna designs play a crucial role in meeting the demands of evolving wireless communication systems, particularly for 5G and beyond. Research in this area remains active, addressing various aspects such as performance enhancement, miniaturization, and cost-effectiveness [25–27]. These studies highlight the significant progress in developing antennas for specific mmWave bands. However, another critical research thrust in multi-band 5G antenna design involves the integration of both sub-6 GHz and mmWave bands into a single system, particularly for user-end devices. Recent works have demonstrated innovative solutions for this co-design challenge, addressing issues of isolation, miniaturization, and co-existence between the different frequency spectrums for smartphone and handset applications [28–30]. While this integration is vital for the advancement of mobile terminals, our study addresses a different but equally important problem. This problem can be summarized as the development of a versatile and reconfigurable antenna operating exclusively within the mmWave spectrum.

This study presents two distinct antenna designs, experimentally tested for 5G operating bands. Both designs incorporate PIN diodes to achieve frequency reconfigurability. The primary mechanism involves electronically altering the antenna's effective electrical structure to selectively activate or deactivate specific operational frequency bands (18, 28, and 38 GHz) and to optimize the in-band impedance matching. This approach focuses on band selection and performance enhancement rather than significant radiation pattern steering. In systems with multiple antennas, such as MIMO and array antennas, PIN diodes can be used to select which antenna is active at a given moment. This functionality is crucial for optimizing signal quality or facilitating the reception of signals originating from diverse spatial orientations. This feature can also be used to control or attenuate the signal strength to or from the antenna. Moreover, for each designated frequency band of operation, PIN diodes facilitate the engagement of pertinent reactive elements, thereby ensuring the appropriate matching of the antenna's input impedance to that particular band. The first design is a four-element array antenna, achieving gains of 6.20 dB, 7.15 dB, and 10.51 dB at 18 GHz, 28 GHz, and 38 GHz, respectively, for a single antenna element. The second design utilizes a 1x4 MIMO antenna array fed by a power divider. These antennas offer reconfigurable operation with bandwidths of 0.80 GHz, 2.62 GHz, and 7.91 GHz at 18 GHz, 28 GHz, and 38 GHz, respectively. Simulations indicate gains of 6.41 dB, 10.33 dB, and 11.70 dB at 18 GHz, 28 GHz, and 38 GHz, respectively, for the reconfigurable antenna. The proposed designs offer advantages over similar studies due to their reconfigurability and high gain, enabling multi-band operation in 5G networks. Furthermore, their operational bandwidths meet 5G network requirements.

2. Design and fabrication of the proposed antennas

This section outlines the design methodology and fabrication process of the two proposed antenna structures. The geometrical parameters were carefully selected to ensure a wide bandwidth, enabling compatibility with 5G communication technologies. The first antenna is designed as a four-element 1 × 4 antenna array. The second MIMO antenna is designed as a four-element cross mirror image array. FR-4 has been employed as the substrate material for the reconfigurable array and MIMO antenna designs. This selection is predicated on a confluence of advantageous properties that render it a widely adopted option in microwave and radio frequency engineering. Firstly, FR-4 offers a favorable balance between its relative permittivity and loss tangent within the frequency bands of interest (18 GHz, 28 GHz, and 38 GHz). Secondly, FR-4 exhibits excellent mechanical characteristics. Its robust flexural and tensile strength, coupled with its ease of machining and processing, simplifies the fabrication and assembly of intricate antenna structures. Thirdly, the cost-effectiveness of FR-4 presents a significant advantage, particularly for prototyping and large-scale production purposes. Finally, the manufacturing processes associated with FR-4 ensure reliable and consistent material properties, which are essential for achieving predictable antenna performance and facilitating the transition from design to fabrication. Both antenna types are reconfigurable within their recommended bandwidths via the utilization of PIN diodes. Specifically, the PIN diodes control designated segments defined by the E_x and E_y parameters presented in Table 1, enabling these segments to be selectively activated or deactivated. This selective switching fundamentally alters the surface current paths and, consequently, the overall electrical length of the radiating structure. This mechanism is strategically employed for two main purposes: (1) to enable or disable resonance at specific frequency bands—for instance, the 18 GHz operation is only possible in one of the diode states—and (2) to optimize the impedance matching and operational bandwidth for the targeted frequency bands, thereby enhancing performance. The reconfigurability is controlled via four integrated PIN diodes. In this study, we focus on two collective operational states: the 'ON' state, where all four diodes are

Table 1
Geometric Parameters of the Proposed Antennas.

Parameter	Value (mm)	Parameter	Value (mm)	Parameter	Value (mm)
Wp	3.47	Ws	1.02	Lf	7.09
Lp	4.29	Wf	1.46	Ls	3.30
Li	0.43	ky	0.20	Lk	1.73
Lii	1.48	kx	0.20	Wi	0.30
La	0.80	Ey	4.00	Mi	5.95
Wa	0.83	Ex	1.30	Mii	6.12

simultaneously activated, and the 'OFF' state, where all four are deactivated. This symmetrical operation is intentionally chosen to maintain the integrity of the radiation pattern and ensure a stable, high-gain main beam, which is critical for the target applications. In this context, the proposed reconfigurable array and MIMO antennas achieve their reconfigurability through the integration and dynamic control of PIN-controlled segments. By selectively activating or deactivating these switching elements through an external bias, the antennas' geometric configurations, and consequently their radiation characteristics, can be dynamically altered.

2.1. Analysis of the Unit-Cell antenna

Prior to evaluating the collective performance of the proposed antenna systems, a comprehensive analysis of the fundamental radiating element is essential. This investigation serves to elucidate the intrinsic operating principles and radiation characteristics that govern the behavior of the larger array and MIMO configurations. The geometric design of this single radiating element, or unit-cell, alongside its physical realization as a fabricated prototype, is depicted in the newly introduced Fig. 1. The analysis will encompass its impedance matching properties via the S_{11} parameter. Establishing this performance baseline is crucial for accurately interpreting the subsequent results and quantifying the enhancements—such as increased directivity and spatial diversity—achieved through the multi-element configurations.

The reconfigurable nature of the antenna is enabled by the integration of PIN diodes, whose operational states are controlled by an external DC bias voltage applied across their terminals. In its "OFF" state, the PIN diode is intended to function as an open circuit, thereby exhibiting high impedance to block the flow of RF current. Ideally, this state is characterized by high isolation and complete signal reflection, which would correspond to a transmission coefficient (S_{21}) approaching $-\infty$ dB and a return loss (S_{11}) of 0 dB, respectively. Conversely, when switched to the "ON" state, the diode approximates a short circuit with low impedance, facilitating maximum current flow along the designated path. In an ideal scenario, this state ensures optimal impedance matching ($S_{11} \to -\infty$ dB) and lossless power transmission ($S_{21} = 0$ dB). It must be noted, however, that in any practical implementation, inherent material properties and diode insertion losses preclude the perfect attainment of these theoretical conditions. The physical structure of the proposed antenna is fabricated on a double-sided FR-4 substrate, characterized by a relative permittivity of 4.3 and a thickness of 0.8 mm. Despite the inherent losses of the FR-4 substrate, which become more pronounced at higher frequencies, the antenna demonstrates acceptable efficiency levels to validate the viability of the proposed reconfigurable topology. It is acknowledged that for commercial applications or systems where maximum efficiency is paramount, employing a low-loss microwave substrate (e.g., Rogers or Taconic) would yield a significant performance improvement. The conductive layers are composed of copper with a thickness of 35 µm. To ensure efficient power delivery to the radiating element, the microstrip feed line, with a length of 3.20 mm and a width of 1.46 mm, has been optimized to achieve a characteristic impedance of 50 Ω.

The comparative performance of the unit-cell antenna is illustrated in Fig. 2, which depicts the simulated and experimentally measured S_{11} parameter for both the "On" and "Off" states of the PIN diodes. The simulation results indicate that the proposed antenna achieves −10 dB impedance bandwidths of 0.797 GHz, 1.939 GHz, and 7.919 GHz centered at the 18 GHz, 28 GHz, and 38 GHz operating frequencies, respectively. Furthermore, the simulated return loss values at these resonant frequencies are exceptionally deep, reaching −60.75 dB, −56.28 dB, and −14.20 dB, which confirms excellent impedance matching in the theoretical design. In comparison, the measurements conducted on the fabricated prototype yield return loss values of −25.43 dB, −12.45 dB, and −14.17 dB at 18 GHz, 28 GHz, and 38 GHz, respectively. As is evident from the results, a good agreement is observed between the simulated and measured data. The minor discrepancies, such as the slight shifts in resonant frequencies and the variation in return loss magnitudes, can be attributed to standard fabrication tolerances and the unavoidable insertion losses associated with the physical connector. It is crucial to note that for all presented analyses, both PIN diodes were operated in the same state (i.e., both 'On' or both 'Off'). This symmetric operation was intentionally maintained to preserve the symmetry of the radiation pattern by ensuring a balanced surface current distribution across the antenna structure.

To further elucidate the fundamental operating mechanism of the unit-cell, the electric field and surface current distributions at each resonant frequency are presented in Fig. 3. The analysis of the surface currents provides a clear physical insight into the multi-band functionality. At 18 GHz (Fig. 3b), the current is distributed over a larger portion of the antenna, including the outer radiating arms, creating a long effective electrical path required for the lower frequency resonance. Conversely, at 28 GHz (Fig. 3d), the current is more concentrated on the central radiating elements. At the highest frequency of 38 GHz (Fig. 3f), the resonance is dominated by the currents on the main feed structure and its immediate vicinity, corresponding to the shortest electrical path. This figures confirm that distinct resonant modes are excited by leveraging different sections of the antenna's geometry, which is the core principle behind its frequency reconfigurable capability.

To fully characterize the fundamental radiation properties, the far-field performance of the unit-cell was also analyzed. Fig. 4 presents the simulated 3D radiation patterns at the three resonant frequencies.

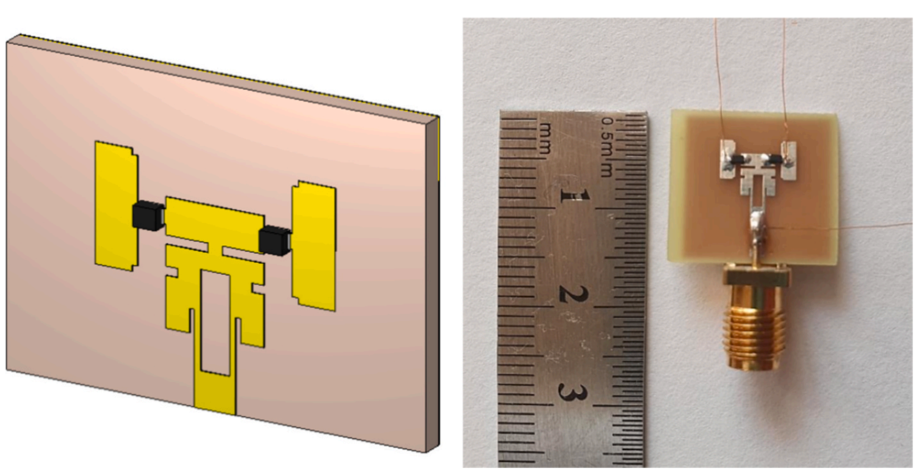

Fig. 1. Perspective view (a) and fabricated view (b) of the proposed unit-cell antenna.

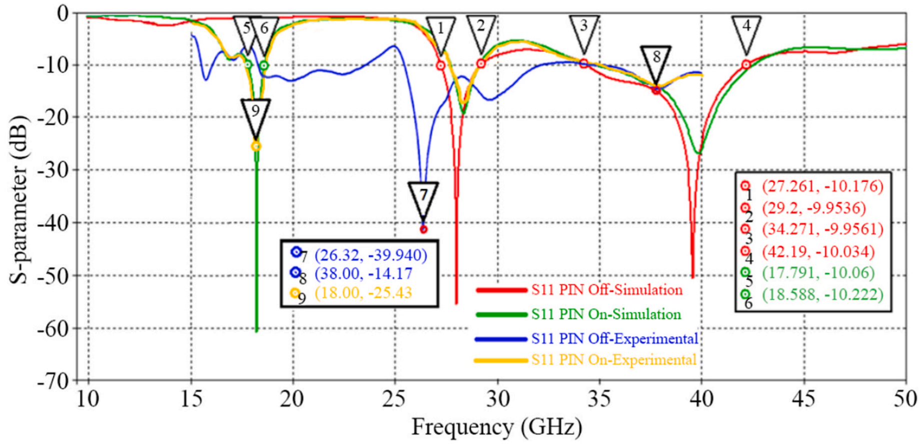

Fig. 2. S_{11} parameter of unit-cell antenna both simulation and experimental.

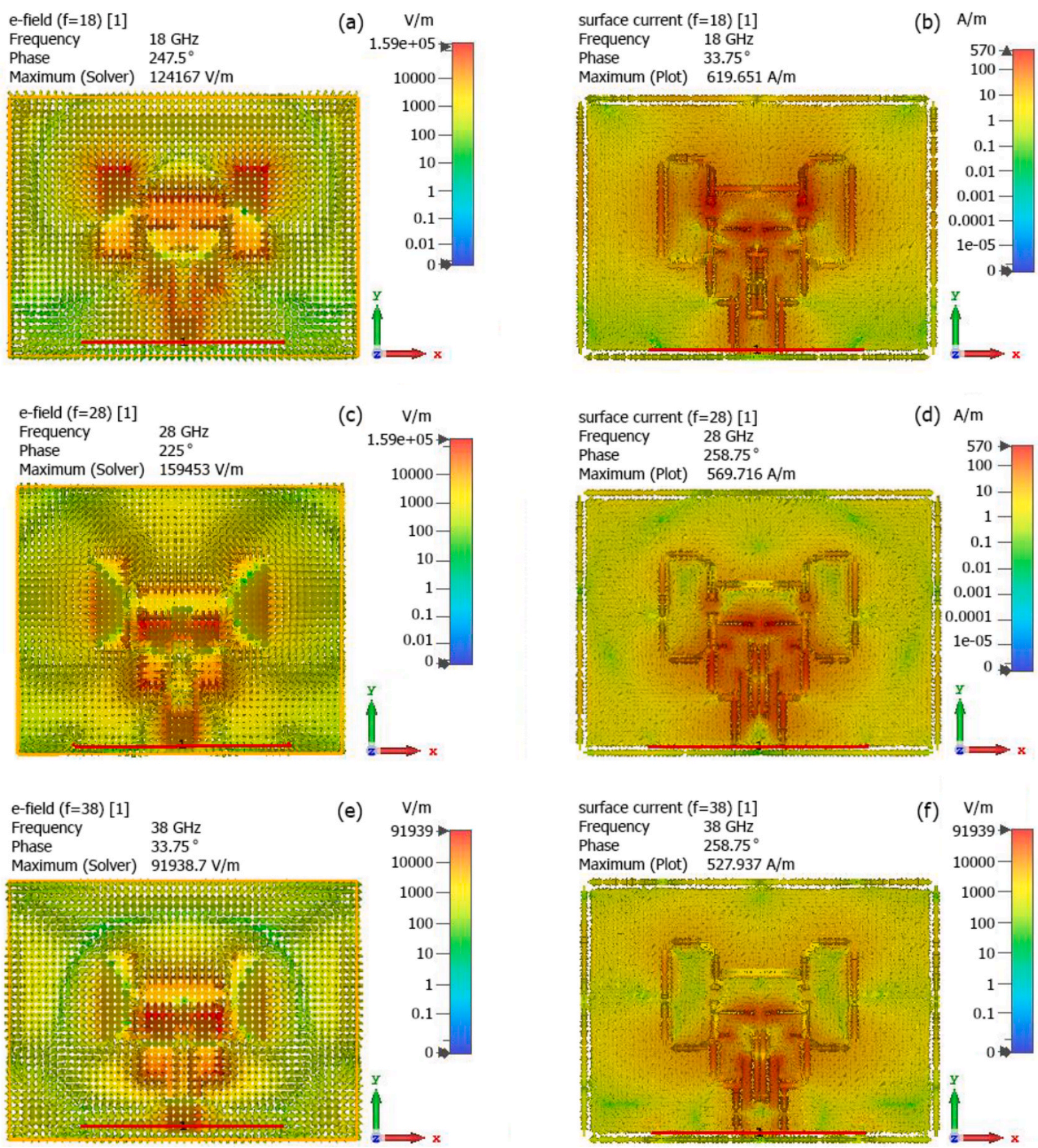

Fig. 3. Simulated electric field and surface current distributions of the unit-cell antenna at its three resonant frequencies: (a, b) 18 GHz, (c, d) 28 GHz, and (e, f) 38 GHz.

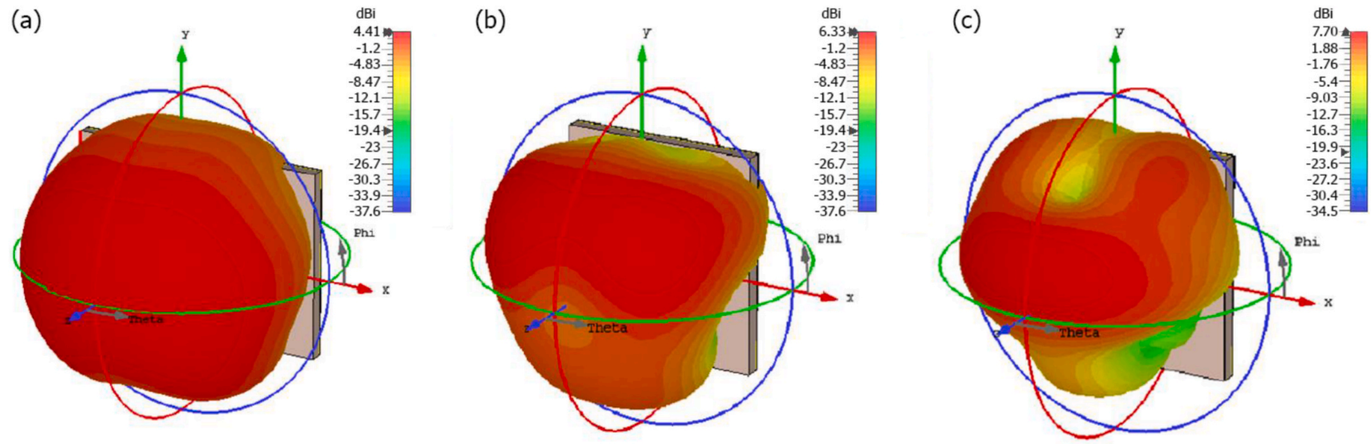

Fig. 4. Simulated 3D radiation patterns of the unit-cell antenna at (a) 18 GHz, (b) 28 GHz, and (c) 38 GHz.

The antenna maintains a stable, broadside radiation pattern across the bands, which is essential for predictable array performance. The quantitative peak gain values are extracted directly from these simulations. The unit-cell achieves peak gains of 4.41 dBi, 6.33 dBi, and 7.70 dBi at 18, 28, and 38 GHz, respectively. It is important to note that peak gain is a function of both the antenna's directivity and its total efficiency. Therefore, these reported gain values inherently include the signal losses attributable to the use of a standard FR-4 substrate. The increasing gain with frequency is consistent with the antenna's electrically larger aperture at higher frequencies, and the results confirm that a reasonable performance is achieved despite the use of a low-cost material, validating the proposed topology for proof-of-concept.

2.2. Design and fabrication of array antenna

An antenna's bandwidth improvement is one of the key requirements for 5G communication applications; however, there are other important parameters to consider. For example, high-gain antenna designs are at the forefront to overcome path loss problems resulting from atmospheric absorption at high frequencies. The proposed antenna designs were created considering such parameters. In this context, a four-element 1 × 4 antenna array has been designed using the power divider feed line method. The proposed array antenna is designed to achieve a multi-band response and a high gain of 10 dBi or more at 5G frequency applications. This antenna comprises four mutually connected antenna elements that function together as a single antenna to transmit/receive electromagnetic waves. In this structure, a feeder energizes each antenna element. The front view and parameters of the unit cell of the proposed antenna are demonstrated in Fig. 5(a). The four antenna elements are positioned to form a 1 × 4 arrangement, which is shown in Fig. 5(b).

The entire array antenna structure is built on a single FR-4 substrate with dimensions of L = 48.43 mm, W = 17.26 mm, and t = 0.8 mm. The FR-4 substrate is characterized by h = 0.8 mm, ε_r = 4.3, and tanδ = 0.002. All unit cell parameters are provided in Table 1. Due to the small size of the antenna elements, the integration of multiple elements leads to high gain and beam steering. The distance between two elements is a critical factor in an array antenna design, as it significantly influences the overall antenna gain. Maximum gain can be achieved in an array antenna design when a spacing of 2λ is maintained between the antenna elements. However, parametric optimization is essential as adhering strictly to a 2λ spacing can substantially increase the array size. Generally, the typical element spacing can be selected between 0.5λ and 2λ. In this study, the element spacing was adjusted to approximately 0.5λ. This value was chosen based on a parametric study which confirmed it as an optimal trade-off to ensure the complete suppression of grating lobes, maintain a compact physical footprint, and manage mutual coupling between the elements at an acceptable level. In the presented antenna design, each antenna element is connected to a 100 Ω microstrip feed line. Two 100 Ω supply lines were joined at a common point, resulting in a 50 Ω impedance. Subsequently, these two common points were reconnected to yield a 50 Ω main feeder impedance. Following the completion of the parametric calculations for the proposed antenna, the fabrication phase commenced. The fabricated reconfigurable array antenna is illustrated in Fig. 5(c).

2.3. Design and fabrication of a MIMO antenna

A MIMO system operates on the principle that a signal transmitted into the channel is broadcast from multiple antennas and subsequently received by multiple antennas upon exiting the channel. The utilization of multiple antennas at both the transmitter and receiver endows the system with signaling degrees of freedom, often referred to as spatial

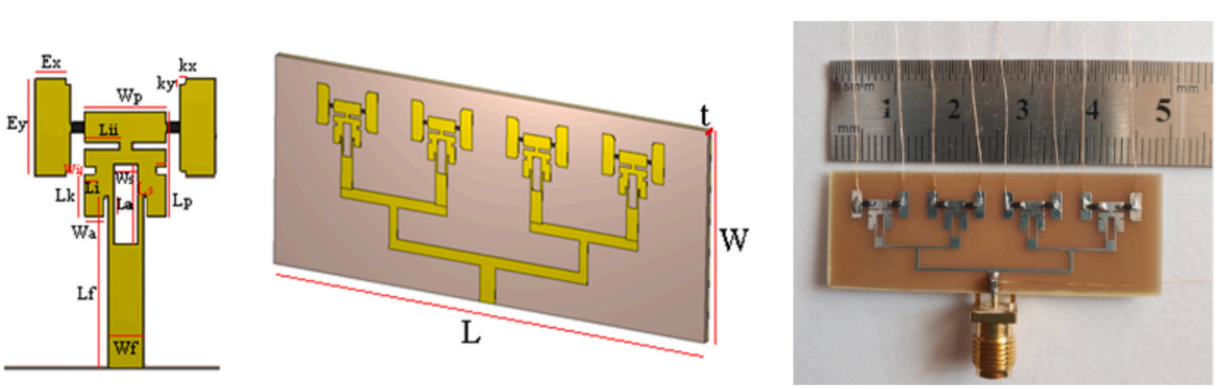

Fig. 5. Front view (a), perspective view (b), and fabricated view (c) of reconfigurable array.

degrees of freedom. Owing to its considerable advantages across numerous aspects, MIMO technology underpins many contemporary telecommunications standards. The proposed MIMO antenna design draws upon these established standards. The initial phase of this work involves the design and geometric optimization of a four-element reconfigurable MIMO antenna intended for K-band radar applications and utilization within 5G communication networks. A broad frequency spectrum spanning 5 to 50 GHz has been selected for the simulation processes. Geometric parameters are then optimized to yield the most suitable frequency peaks within the defined frequency range. To achieve frequency reconfigurability, the MA4AGFCP910 PIN diode, supplied by MACOM, was utilized in the design. The selection was based on its favorable performance characteristics at high frequencies and its compact form factor suitable for integration. For accurate prediction of the antenna's behavior, the diode was modeled in the simulation environment using a lumped element equivalent circuit derived from the manufacturer's datasheet. In its forward biased "ON" state, the diode is represented by a series resistance (R_s) of 4.2 Ω and a series inductance of 0.5 nH. Conversely, in its reverse biased "OFF" state, the model consists of a parallel junction capacitance of 20 fF and a shunt resistance of 3 kΩ. This detailed modeling is critical for accurately simulating the switched current paths and predicting the antenna's reconfigurable performance across the target frequency bands.

The resultant design, derived from the optimized parameters, is illustrated in Fig. 6(a). Antenna elements are positioned in a 2 × 2 configuration, with each adjacent element rotated by 90°. Furthermore, the inter-element spacing has undergone optimization. This configuration ensures enhanced isolation between neighboring elements and improves the overall return loss profile of the antenna. The proposed MIMO antenna structure is built on a single substrate of FR-4 material, occupying a volume of 29.30 × 29.30 × 0.8 mm^3. This FR-4 substrate possesses identical parametric values to the material employed in the array antenna design. All optimized parameters of the proposed antenna are detailed in Table 1. Following the completion of the optimization process, the attainment of the targeted performance is observed, and subsequently, the fabrication process is initiated. The fabricated antenna prototype is depicted in Fig. 6(b). The simulation and fabrication phases of the proposed antenna are planned with consideration for multi-channel characteristics. In addition to its multi-channel capability, the antenna can operate across different frequency bands simultaneously by adjusting the antenna elements at varying frequencies, thereby enhancing the versatility of this MIMO configuration.

3. Simulation and experimental results

Following the obtaining of suitable geometric parameters for the proposed array antenna and MIMO antenna, both simulation and experimental results were investigated. This section initially details the calculation of the scattering parameters (S-parameters) for the proposed antennas. Subsequently, the measurement of the S-parameters for the fabricated antennas was conducted. Finally, the results obtained were compared and evaluated. To provide a standardized and more meaningful metric for comparing antenna performance across different frequency bands, all reported bandwidths in this study have been presented to include their corresponding fractional bandwidth (FBW). The FBW is calculated using the formula: FBW (%) = [(f_upper − f_lower) / f_center] × 100, where f_upper and f_lower denote the upper and lower −10 dB frequencies, and f_center is the resonant frequency of the band.

3.1. Reconfigurable array antenna

The scattering parameters (S-parameters) serve as a fundamental metric for evaluating antenna performance, providing insights into reflected and transmitted power. These S-parameters, also referred to as the S-matrix, are employed to characterize the linear behavior of components, including electronic circuits and electromagnetic materials. Utilizing the S-parameter matrix, key properties such as loss, gain, impedance, voltage standing wave ratio (VSWR), and group delay can be determined. A lower value of the S_{11} parameter generally indicates improved antenna resonance. Furthermore, the operating frequency and bandwidth of the antenna are ascertained from the return loss plot. The S_{11} plot of the frequency reconfigurable array antenna is presented in Fig. 7, illustrating both simulated and measured data for the "Off" and "On" states of the PIN diodes. Simulation studies were conducted within the frequency range of 10–50 GHz, while measurements were performed within the 15–40 GHz range.

In Fig. 7, six points at the −10 dB reference level were identified to analyze the bandwidths of the proposed antenna. These six points encompass the PIN diode's "Off" and "On" states for both simulation and experimental data, and they correspond to frequencies of 18, 28, and 38 GHz. At the 18 GHz frequency, the proposed antenna exhibits bandwidths of 0.75 GHz (4.1 % FBW) (17.87–18.62 GHz, On-Simulation), no data (Off-Simulation), 1.02 GHz (5.6 % FBW) (17.64–18.66 GHz, On-Experimental), and 0.54 GHz (3.0 % FBW) (17.71–18.25 GHz, Off-Experimental), based on PIN diode "On/Off" states in simulation and experimental measurements, respectively. The widest bandwidth at 18 GHz is observed for the PIN "On"-experimental S_{11} parameter. Considering the 28 GHz frequency, bandwidths of 1.82 GHz (6.4 % FBW) (27.46–29.28 GHz), 2.69 GHz (9.5 % FBW) (26.89–29.58 GHz), 0.98 GHz (3.5 % FBW) (27.45–28.43 GHz), and 1.63 GHz (5.8 % FBW) (27.18–28.81 GHz) were obtained for the PIN diode "On/Off" states in simulation and experimental measurements, respectively. The widest bandwidth at 28 GHz is the PIN "Off"-simulation S_{11} parameter. For the 38 GHz frequency, Points five and six, which exhibit the widest bandwidths, were considered. At this frequency, the proposed antenna achieves bandwidths of 7.63 GHz (19.5 % FBW) (35.32–42.95 GHz), 7.59

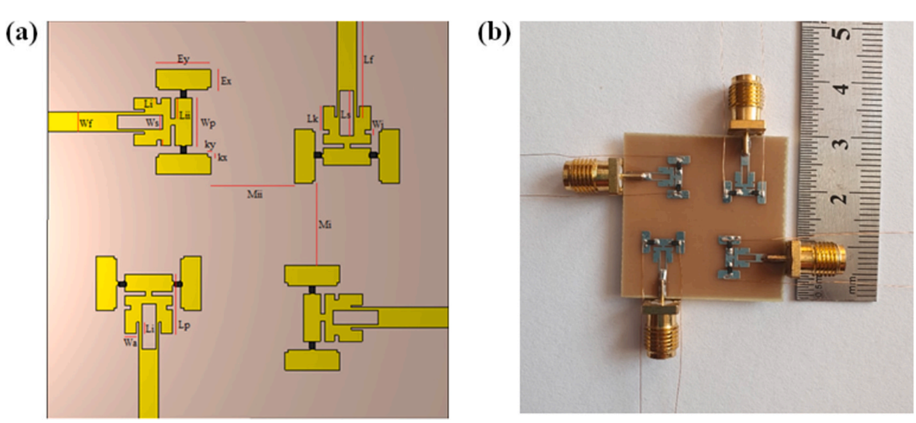

Fig. 6. Perspective (a) and fabrication (b) view of the proposed reconfigurable 2 × 2 MIMO antenna with geometric dimension.

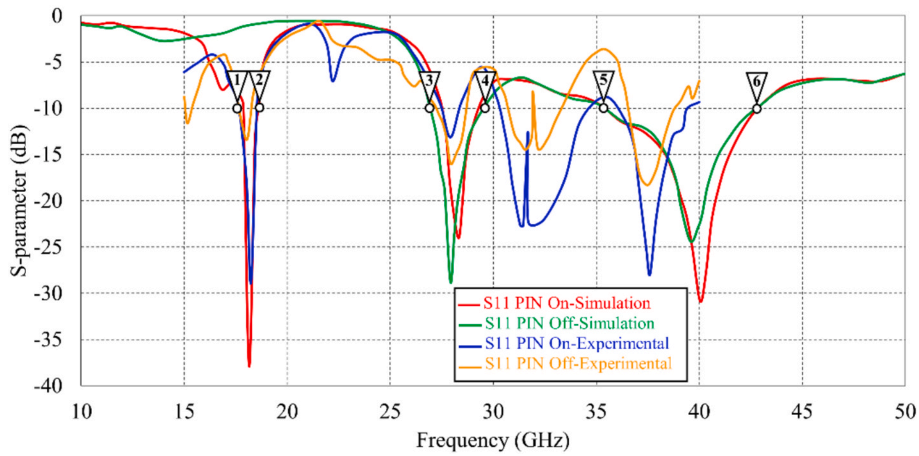

Fig. 7. S_{11} parameter of reconfigurable array antenna both the simulation and experimental.

GHz (19.4 % FBW) (35.32–42.91 GHz), 3.37 GHz (8.9 % FBW) (36.02–39.39 GHz), and 2.26 GHz (6.0 % FBW) (36.52–38.78 GHz) for the respective PIN diode states and data types. Notably, the PIN "On/Off" simulation values are remarkably high at 38 GHz, and the PIN "On"-experimental bandwidth reaches its maximum of 3.37 GHz. The good agreement between the simulated and measured data validates the design; however, minor discrepancies are observable. These deviations, such as slight shifts in resonant frequencies and variations in return loss magnitudes, are attributed to a combination of practical factors including standard fabrication tolerances in the etching process, slight variations in the FR-4 substrate's dielectric constant, and the unavoidable parasitic effects introduced by the manual soldering of the PIN diodes and the input connector. A noteworthy example of these practical effects is the weak resonance observed at 18 GHz in the 'OFF' state of the array antenna (Fig. 7), which deviates from the ideal simulation. This is primarily attributed to parasitic capacitive coupling within the more complex 1x4 power divider feed network. However, it is critical to distinguish this shallow, poorly matched resonance ($S_{11} \approx -11$ dB) from the deep, well-matched resonance achieved in the 'ON' state. From a practical system standpoint, the 18 GHz band is only considered effectively operational when the diodes are activated, thus validating the reconfigurable nature of the array.

In order to explain the physical behavior of the proposed antenna structure, the electric field and surface current distributions were analyzed at a frequency of 28 GHz. Fig. 8(a) illustrates the electric field distribution at the 28 GHz resonant frequency, while Fig. 8(b) depicts the surface current distribution at the same frequency. The electric field distributions at 28 GHz are presented within a range of 0 to 43134.6 V/m. The surface current distribution at 28 GHz was observed within a range of 0 to 277.98 A/m. As depicted in Fig. 8(a), the electric field is primarily concentrated on the transmission lines of the array antenna, particularly along the x-direction. Similar to the electric field, the surface current is predominantly accumulated on the transmission lines of the proposed antenna. Concurrently, some surface current concentration

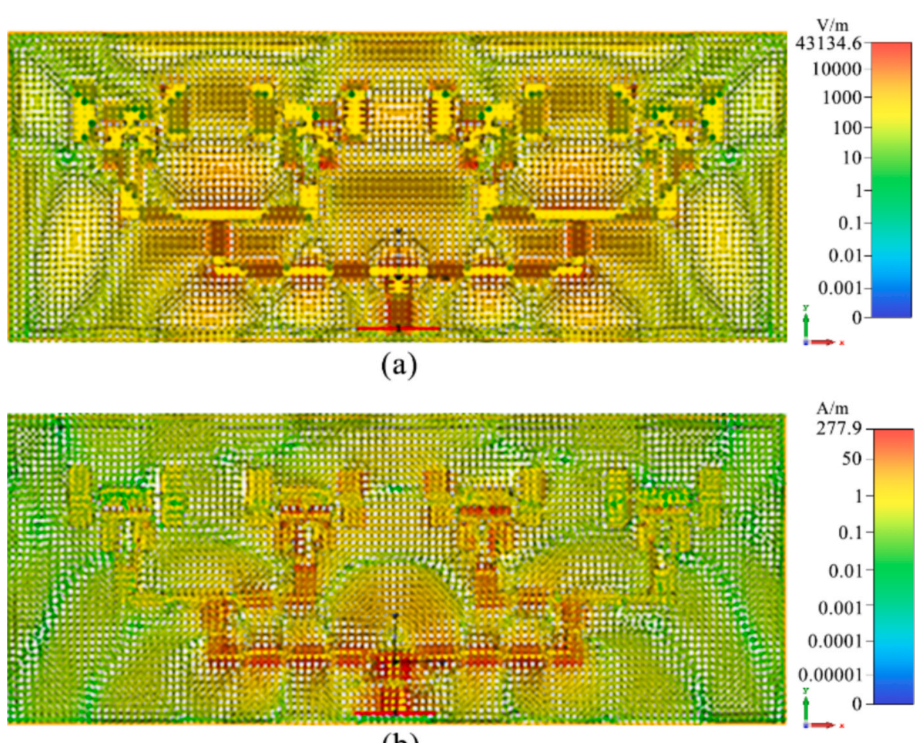

Fig. 8. Electric field distribution (a) and surface current distribution (b) of proposed array antenna at 28 GHz.

is also evident in the central regions of the array antenna.

The three-dimensional representation of the power radiated by the designed antenna in free space constitutes the three-dimensional (3D) radiation pattern, typically measured in the far-field region. In other words, it quantifies the power radiated in a specific direction relative to an isotropic radiator. Analysis of the 3D radiation pattern allows for the observation of the power transmitted by the antenna in a given direction. Fig. 9 presents the 3D radiation patterns of the reconfigurable array antenna. According to the simulation results for the proposed reconfigurable antenna, gain values of 6.41-, 10.33–, and 11.70-dB were obtained at 18, 28, and 38 GHz, respectively.

3.2. Reconfigurable MIMO antenna

In this section, the simulation and experimental results of the reconfigurable MIMO antenna are analyzed. Initially, the performance of the proposed antenna was evaluated through a parametric study, and subsequently, the measurements were validated by developing a prototype of the designed antenna. The simulation results were obtained through eight different calculations, considering four PIN diode states (on and off). The measurement results were conducted for two states: PIN on and off. The reflection coefficient results derived from both simulation and experimental studies are presented in Fig. 10. The measured S-parameters of the prototype closely align with the simulated results, with minor discrepancies attributed to manufacturing tolerances and connector losses.

The simulation and measurement studies of the proposed MIMO antenna were conducted in the frequency ranges of 10–50 GHz and 15–40 GHz, respectively. In Fig. 10, three points are marked at 18, 28, and 38 GHz. Due to the symmetrical design of the structure, the performance of all four ports (S_{11}, S_{22}, S_{33}, and S_{44}) is nearly identical. In this respect, the results are evaluated as S11. The first point, corresponding to 18 GHz, lies on the S_{11} PIN-On experimental data curve and has a magnitude of –22.34 dB, which is below −10 dB. Additionally, the bandwidth at 18 GHz, determined based on the −10 dB threshold in the PIN-On experimental data, spans the frequency range of 16.36–18.53 GHz, corresponding to a fractional bandwidth of 12.4 %. The second point, representing 28 GHz, lies on the S_{11} PIN-On experimental data curve with a magnitude of −20.03 dB and a bandwidth of 25.43–33.87 GHz, based on the −10 dB threshold. The bandwidths at 18 GHz and 28 GHz in the PIN-On mode are 2.17 GHz (12.4 % FBW) and 8.44 GHz (28.5 % FBW), respectively, with the 28 GHz bandwidth being remarkably wide. The experimental data for S_{11} in PIN-Off mode, which has a lower value than the PIN-On mode, shows a magnitude of −16.95 dB at 28 GHz. The third point corresponds to 38 GHz. According to the S_{11} PIN-Off experimental data, the magnitude at 38 GHz is −16.66 dB, with a bandwidth of 0.51 GHz (1.3 % FBW) in the 37.79–38.30 GHz range based on the −10 dB threshold. In the PIN-On mode, the experimental data indicate a magnitude of −6.63 dB at 38 GHz, which remains below −10 dB. Examining the simulation results, the S_{11} PIN-Off data show no peak at 18 GHz. However, across all PIN-Off simulation data, peaks are observed around 28 GHz and 38 GHz. The minimum magnitude values at 28 GHz and 38 GHz are –33.71 dB and −27.05 dB, respectively. When the PIN-On mode is activated, simulation results show peaks at 18, 28, and 38 GHz, with minimum magnitude values of −27.25 dB, −16.66 dB, and −58.03 dB, respectively. While the proposed MIMO antenna does not generate a peak at 18 GHz in PIN-Off mode, it exhibits a peak at 18 GHz when switched to PIN-On mode.

In the proposed design, the transmission coefficients between the antennas remain below −25 dB for both states of the PIN diode, as shown in Fig. 11. The experimental results for the S_{21} coefficient at 18 GHz in the PIN-On mode are presented in Fig. 11(a), while Fig. 11(b) illustrates the experimental results for the S_{21} coefficient at 28 GHz and 38 GHz in the PIN-Off mode. To ensure minimal interference and high isolation between the antenna elements, the transmission coefficient should be at least below −10 dB. The results indicate that this criterion is met at 18 GHz, 28 GHz, and 38 GHz, confirming that the MIMO antenna can operate efficiently across different frequencies.

In MIMO antenna structures, minimizing the mutual coupling between individual radiating elements is crucial. This is essential to mitigate signal losses. In the presented design, adjacent antennas are positioned orthogonally with an inter-element spacing of $\lambda/2$ to achieve isolation. Fig. 12 illustrates the electric field distribution and surface current distribution at 28 GHz, the designated operating frequency of the antenna when ‘Port 1′ is excited. As evident from the figure, the electric current is predominantly concentrated around the slot on the feed line. The maximum surface current density observed on the antenna element is 495 A/m. Furthermore, due to the orthogonal positioning and the $\lambda/2$ separation between the antennas, it is seen that the antenna activated with ‘Port 1′ has a small influence on the other elements.

Finally, the 3D radiation pattern of the proposed MIMO antenna design is examined. The 3D radiation patterns of the antenna structure at 18 GHz, 28 GHz, and 38 GHz are depicted in Fig. 13. In a reconfigurable MIMO antenna, the gain values for a single antenna element at the frequencies of 18 GHz, 28 GHz, and 38 GHz are 6.20 dB, 7.15 dB, and 10.51 dB, respectively. In MIMO antennas, each antenna element operates independently. Therefore, characterizing the gain of an individual element is of greater significance than the overall array gain of the general MIMO scheme. A comparison of the presented MIMO antenna with a single antenna reveals the preservation of the operating frequencies. Furthermore, the gain exhibits an increase from 4.41 dB to 6.20 dB at 18 GHz, from 6.63 dB to 7.15 dB at 28 GHz, and from 7.70 dB to 10.51 dB at the 38 GHz operating frequency in the MIMO antenna configuration. The reconfigurable MIMO antenna structure demonstrates a notable enhancement in gain, alongside the achievement of multi-channel transmission capabilities.

The frequency bands of 18 GHz, 28 GHz, and 38 GHz are significant within the context of modern wireless communication systems, particularly for the burgeoning field of 5G and beyond. Reconfigurable array and MIMO antenna technologies operating within these bands have

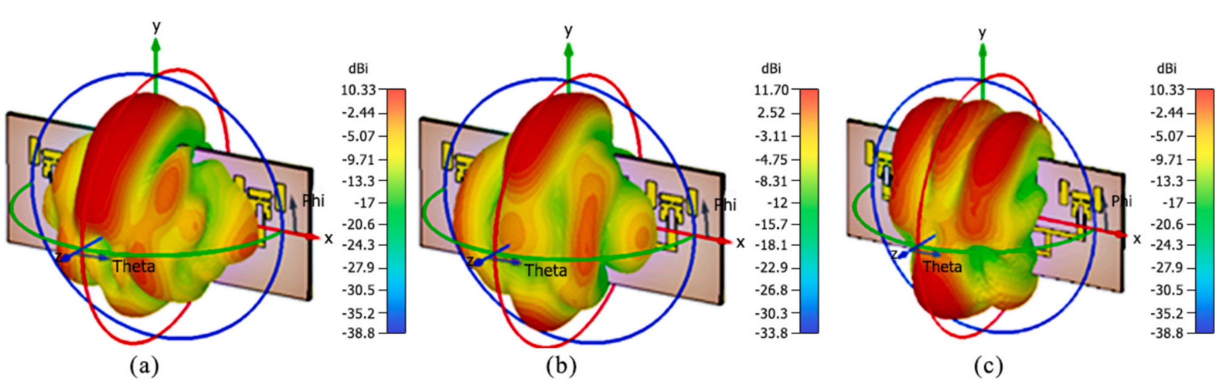

Fig. 9. 3D radiation patterns of proposed array antenna at 28 GHz and PIN-Off diode (a), 38 GHz and PIN-Off diode (b), and 18 GHz and PIN-On diode (c).

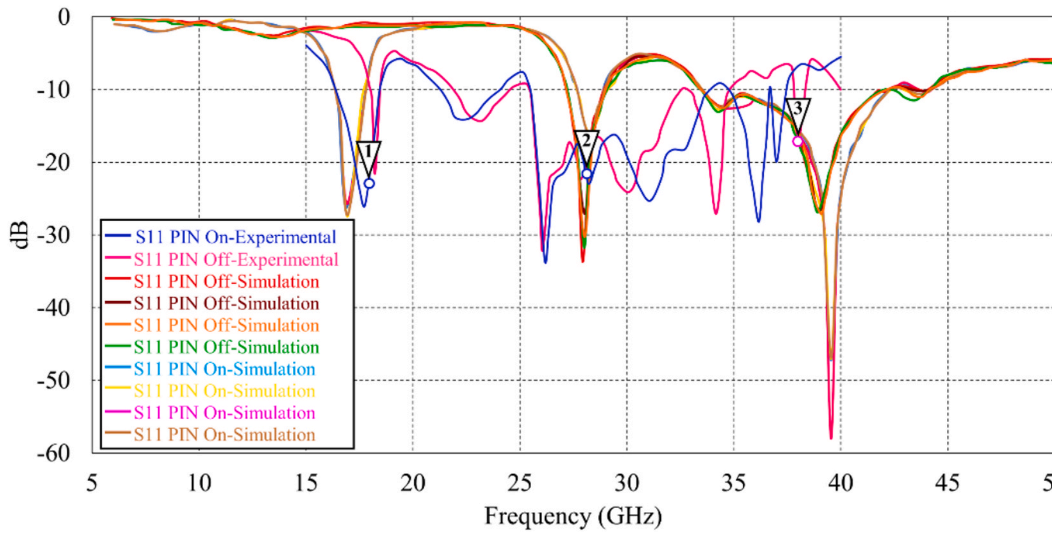

Fig. 10. Reconfigurable MIMO antenna's $S_{ii}(i = 1 - 4)$ parameters for simulation and measurement studies.

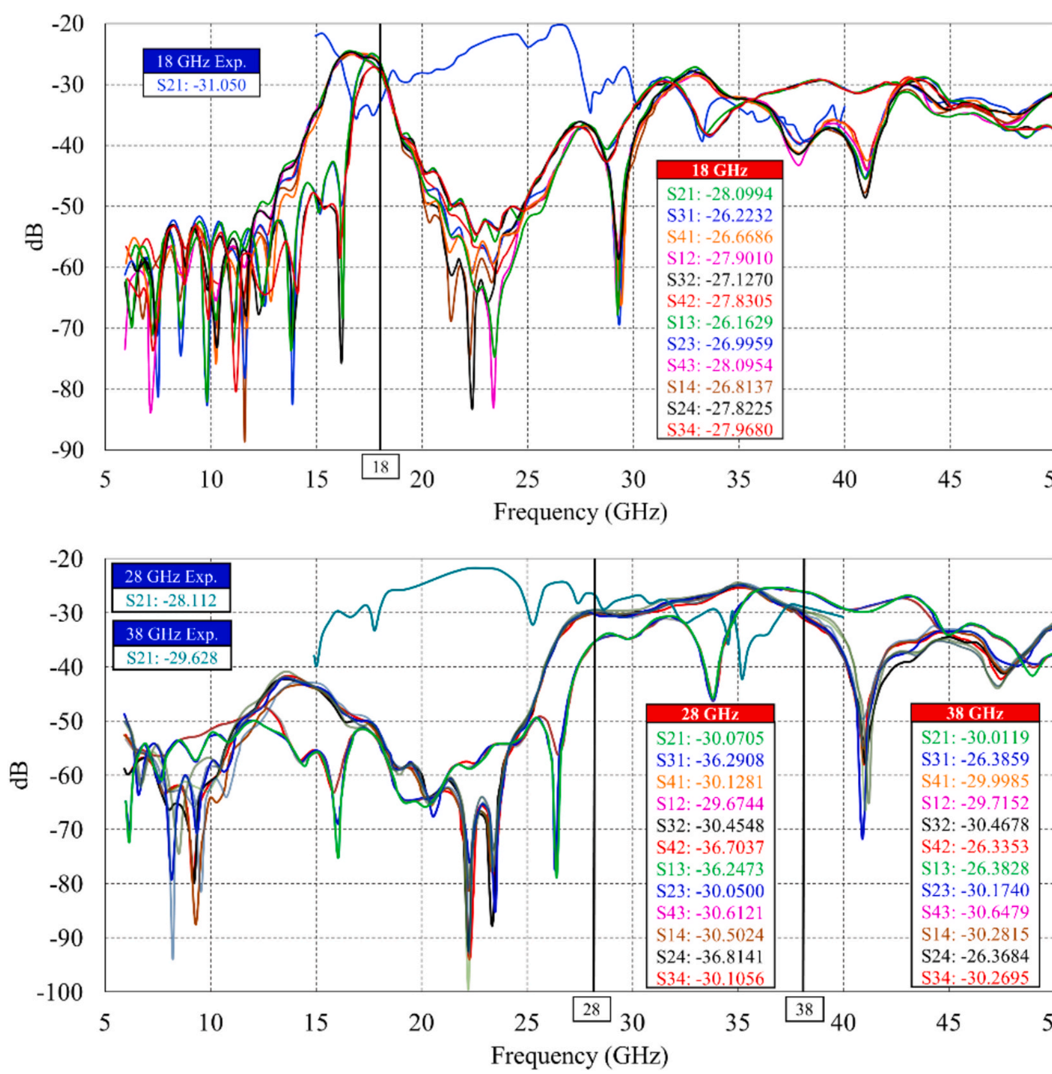

Fig. 11. Transmission coefficients of reconfigurable MIMO antenna for all ports at 18 GHz (a), 28 GHz and 38 GHz (b) according to the simulation and experimental data.

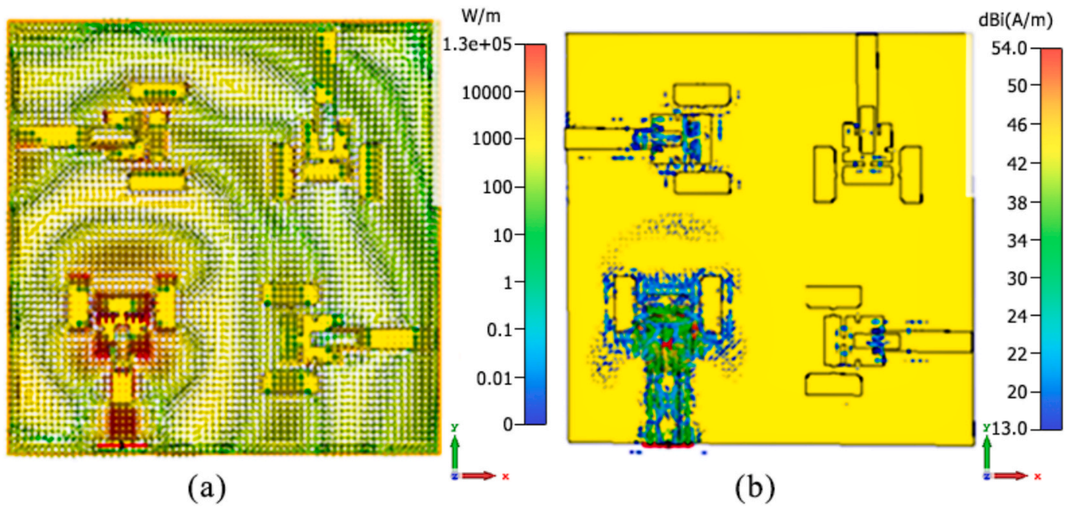

Fig. 12. (a) Electric Field and (b) current distribution of reconfigurable MIMO antenna at 28 GHz frequency.

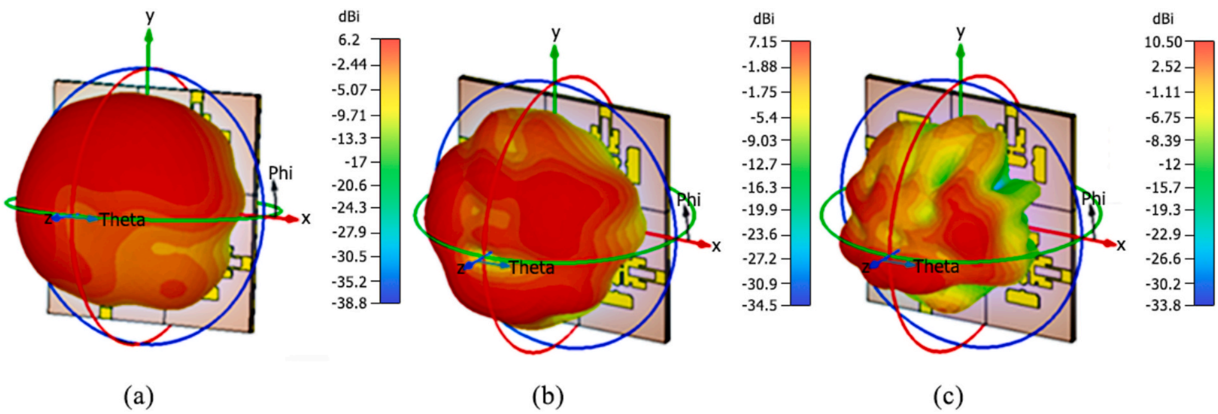

Fig. 13. Proposed reconfigurable MIMO antenna's 3D radiation pattern at (a) 18, (b) 28, and (c) 38 GHz frequency.

advantages due to their ability to dynamically adapt their radiation characteristics and enhance spectral efficiency. Reconfigurable array antennas are used for beam steering and tracking to overcome the high path loss and susceptibility to blockage inherent at mmWave frequencies. Additionally, by forming multiple narrow beams, they can effectively increase the coverage area. Beam steering capabilities enable robust point-to-point links, bypassing obstacles and optimizing signal strength. It is also widely used in radar applications such as K-band (18–26.5 GHz) and Ka-band (26.5–40 GHz). MIMO antenna systems, employing multiple transmit and receive antennas to exploit spatial diversity and spatial multiplexing, offer significant benefits at 18 GHz, 28 GHz, and 38 GHz. Spatial multiplexing in MIMO systems enables the transmission of multiple data streams simultaneously over the same frequency band, significantly increasing data rate. Additionally, it provides improved link reliability and robustness. Reconfigurability allows the MIMO system to dynamically adjust the number of spatial streams, and the diversity scheme based on channel conditions. Reconfigurable elements can enable the antenna to operate across different frequency bands or support different communication modes, providing versatility for future wireless systems.

4. Discussion

Given their inherent capabilities in beam steering, spatial multiplexing, and dynamic adaptability within the significant 18 GHz, 28 GHz, and 38 GHz frequency bands, the proposed reconfigurable array and MIMO antenna technologies hold considerable promise for a multitude of advanced wireless applications. The demonstrated ability of the proposed reconfigurable array antenna to manipulate radiation patterns effectively addresses the challenges of signal propagation at mmWave frequencies, enabling reliable communication links for high-capacity data transmission and radar systems. Furthermore, the inherent capacity of the proposed MIMO antenna system to enhance data rates and link reliability through spatial diversity and multiplexing directly supports the demanding requirements of next-generation wireless networks, including increased throughput and seamless connectivity.

Having established the simulated and experimental performance of the proposed reconfigurable antennas in the preceding sections, the subsequent step is to contextualize these findings and evaluate the contribution of this work within the broader field. To this end, this section provides a direct comparison with several millimeter-wave antennas reported in recent literature. A comprehensive benchmark is presented in Table 2, focusing on key performance metrics such as operational frequencies, reconfiguration type, peak gain, and substrate material. This comparative analysis serves to provide a clear and quantitative basis for highlighting the novelty and specific advantages of the proposed designs. Firstly, the antenna's unique triple-band reconfigurability (18/28/38 GHz) offers unparalleled versatility, enabling multi-functional operation from a single, compact aperture. Furthermore, achieving this high-gain performance on a low-cost FR-4 substrate marks a significant practical achievement, paving the way for cost-

Table 2
Comparison of technical specifications with existing designs.

Ref.	Year	Freq. (GHz)	Reconfig. Type	Peak Gain (dBi)	Substrate	Dimensions (mm^2)	Key Feature
[13]	2020	28/37.3	Dual-Band (Fixed)	7.9/13.7	Rogers RO4003C	30 x 14	Yagi-Uda design, high gain, not reconfigurable.
[20]	2022	27/39	Dual-Band (Fixed)	5.0/5.7	Rogers RO4350B	40 x 40	Uses expensive substrate, not reconfigurable.
[21]	2021	28/38	Dual-Band (Fixed)	7.4/8.5	Rogers RO5880	25 x 30	Compact, but not reconfigurable.
[31]	2023	28/38	Freq. Reconfig.	6.5/7.4	Duroid 5880	10 x10	Reconfigurable, expensive substrate.
[32]	2023	28/38	Freq. Reconfig.	7.16/10	Roger 5880	15x10	Reconfigurable, high gain, expensive substrate, either 28 or 38 GHz; not both.
This Work	2025	18/28/38	Freq. Reconfig.	6.4/10.3/11.7 (Array)6.2/7.2/10.5 (MIMO)	FR-4	30 x 30	Triple-band operation on low-cost substrate with simple control, high gain.

effective mass production. This multi-band capability is governed by a remarkably simple control mechanism, which enhances system reliability and eases integration. Ultimately, this work presents a compelling and well-balanced solution, successfully combining multi-band operation, high gain, and cost-effectiveness, a combination not easily found in contemporary designs.

5. Conclusion

This study presents the design of two antenna types intended for the operating frequency range of contemporary 5G technologies. The first design comprises a four-element 1×4 antenna array utilizing the power divider feedline technique. The second design is a reconfigurable MIMO antenna featuring a four-element cross-mirror image configuration. Both antenna designs were undertaken with a focus on enhancing bandwidth, a critical parameter for 5G communication applications. Furthermore, the proposed antennas were optimized to achieve high gain, aiming to mitigate path losses resulting from atmospheric absorption at elevated frequencies. Initially, the geometric parameters of both proposed antennas were optimized to yield efficient S-parameter values. Subsequently, the fabrication phase was executed, and the experimental results were compared with simulations. Calculations and measurements were performed at 18, 28, and 38 GHz frequencies. Crucially, the study validates the core principle of frequency reconfigurability by demonstrating effective band switching. This is best exemplified by the MIMO antenna (Fig. 8), where the 18 GHz band is cleanly activated only in the ’ON’ state, aligning perfectly with simulations and validating the unit-cell’s design. While the array antenna’s more complex feed network introduced a weak parasitic resonance in the ’OFF’ state (Fig. 5), its poor matching quality confirms that efficient operation at 18 GHz remains exclusive to the ’ON’ state. Furthermore, the ability to optimize in-band performance, as seen by the differing bandwidths at 28 GHz between diode states, underscores the advantage of this active reconfigurable approach over static multi-band designs. The obtained results indicate that the proposed array antenna exhibits bandwidths of 0.80 GHz at 18 GHz, 2.62 GHz at 28 GHz, and 7.91 GHz at 38 GHz. These values suggest that the array antenna design is capable of operating within all FCC-reported millimeter-wave (MMW) 5G bands. The results obtained from the designed MIMO antenna demonstrate a transmission coefficient below −25 dB. In conclusion, this study has successfully presented the design and experimental validation of two reconfigurable antenna types operating effectively at 18, 28, and 38 GHz. The consistency between simulation and measurement confirms their viability for practical implementation. Beyond their individual performance metrics, the significance of these antennas lies in their potential to enable highly integrated, multi-functional systems. As demonstrated, a single aperture can be dynamically reconfigured to support diverse applications—from 5G mobile access and wireless backhaul to K-band radar sensing. This capability directly addresses the need for reduced SWaP-C (Size, Weight, Power, and Cost) in next-generation wireless infrastructure, positioning the proposed designs as compelling candidates for deployment in smart city nodes, autonomous vehicles, and adaptive small cells. Consequently, the development and optimization of such reconfigurable array and MIMO antenna designs are crucial for realizing the full potential of emerging wireless communication and sensing paradigms.

Declarations

Ethical Approval

This article does not contain any studies with animals performed by any of the authors.

CRediT authorship contribution statement

Halil Paşalıoğlu: Writing – original draft, Software, Methodology. **Lulu Wang:** Investigation, Formal analysis, Data curation. **Mehmet Bakır:** Writing – review & editing, Resources, Data curation. **Liton Chandra Paul:** Writing – original draft. **Erkan Tetik:** Writing – review & editing, Writing – original draft, Validation. **Muharrem Karaaslan:** Writing – review & editing, Writing – original draft, Validation, Data curation.

Funding

None.

Declaration of competing interest

The authors declare that they have no known competing financial interests or personal relationships that could have appeared to influence the work reported in this paper.

Acknowledgments

The authors declare that they received no specific funding and have no acknowledgments to disclose related to this study.

Data availability

No data was used for the research described in the article.

References

[1] M.H. Sharaf, A.I. Zaki, R.K. Hamad, M.M.M. Oma, A novel dual-band (38/60 ghz) patch antenna for 5g mobile handsets, Sensors (Switzerland) 20 (9) (2020) 2541, https://doi.org/10.3390/s20092541.

[2] N.M. Rashad, A.I. Hussein, A.A.M. Khalaf, Two-Element Pharaonic Ankh-Key Array Antenna Design, simulation, and Fabrication for 5G and Millimeter-Wave Broadband applications, IEEE Access 10 (2022) 15175–15182, https://doi.org/10.1109/ACCESS.2022.3148589.

[3] P.A. Dzagbletey, Y.B. Jung, Stacked microstrip linear array for millimeter-wave 5G baseband communication, IEEE Antennas Wirel. Propag. Lett. 17 (5) (2018) 780–783, https://doi.org/10.1109/LAWP.2018.2816258.

[4] S. Chaudhary, A. Kansal, Compact high gain 28, 38 GHz antenna for 5G communication, Int. J. Electron. 110 (6) (2023) 1028–1048, https://doi.org/10.1080/00207217.2022.2068201.

[5] J. Saini, S.K. Agarwal, Design a single band microstrip patch antenna at 60 GHz millimeter wave for 5G application, in: In: 2017 International Conference on Computer, Communications and Electronics (COMPTELIX 2017), 2017, pp. 227–230, https://doi.org/10.1109/COMPTELIX.2017.8003969.
[6] Y. Xu, G. Gui, H. Gacanin, F. Adachi, A Survey on Resource Allocation for 5G Heterogeneous Networks: Current Research, Future Trends, and Challenges, IEEE Communications Surveys and Tutorials 23 (2) (2021) 668–695, https://doi.org/10.1109/COMST.2021.3059896.
[7] M. Hussain, W.A. Awan, E.M. Ali, M.S. Alzaidi, M. Alsharef, D.H. Elkamchouchi, A. Alzahrani, M. Fathy Abo Sree, Isolation Improvement of Parasitic Element-Loaded Dual-Band MIMO Antenna for Mm-Wave applications, Micromachines (basel) 13 (11) (2022), https://doi.org/10.3390/mi13111918.
[8] M. Sangwan, G. Panda, P. Yadav, A Literature Survey on Different MIMO Patch Antenna, in: Proceedings of the 5th International Conference on Inventive Computation Technologies (ICICT 2020) 2020 912-918, doi: 10.1109/ICICT48043.2020.9112566.
[9] A. Khabba, J. Amadid, S. Mohapatra, Z. El Ouadi, S. Ahmad, S. Ibnyaich, A. Zeroual, UWB dual-port self-decoupled o-shaped monopole MIMO antenna with small-size easily extendable design and high diversity performance for millimeter-wave 5G applications, Appl. Phys. A Mater. Sci. Process. 128 (2022) 725, https://doi.org/10.1007/s00339-022-05881-7.
[10] M. Venkateswara Rao, B.T.P. Madhav, J. Krishna, Y. Usha Devi, T. Anilkumar, B. Prudhvi Nadh, CSRR-loaded T-shaped MIMO antenna for 5G cellular networks and vehicular communications, Int. J. RF Microwave Comput. Aided Eng. 29 (8) (2019) e21799, https://doi.org/10.1002/mmce.21799.
[11] S.M. Shamim, U.S. Dina, N. Arafin, S. Sultana, Design of Efficient 37 GHz Millimeter Wave Microstrip Patch Antenna for 5G Mobile Application, Plasmonics 16 (2021) 1417–1425, https://doi.org/10.1007/s11468-021-01412-x.
[12] N. Ojaroudi Parchin, H. Jahanbakhsh Basherlou, Y. I A Al-Yasir, A. M Abdulkhaleq, R. A Abd-Alhameed, Ultra-Wideband Diversity MIMO Antenna System for Future Mobile Handsets, Sensors (Basel) 20(8) (2020) 2371, doi: 10.3390/s20082371.
[13] A.E. Farahat, K.F.A. Hussein, 28/38 GHz dual-band Yagi-Uda antenna with corrugated radiator and enhanced reflectors for 5g MIMO antenna systems, Progress in Electromagnetics Research C 101 (2020) 159–172, https://doi.org/10.2528/PIERC20022603.
[14] D. Wen, Y. Hao, H. Wang, H. Zhou, Design of a MIMO Antenna with High Isolation for Smartwatch applications using the Theory of Characteristic Modes, IEEE Trans. Antennas Propag. 67 (3) (2019) 1437–1447, https://doi.org/10.1109/TAP.2018.2884849.
[15] M. Khalid, S.I. Naqvi, N. Hussain, M.U. Rahman, Fawad, S.S. Mirjavadi, M.J. Khan, Y. Amin, 4-port MIMO antenna with defected ground structure for 5G millimeter wave applications, Electronics (Switzerland) 9(1) (2020) 71, doi: 10.3390/electronics9010071.
[16] D.A. Sehrai, M. Asif, N. Shoaib, M. Ibrar, S. Jan, M. Alibakhshikenari, A. Lalbakhsh, E. Limiti, Compact quad-element high-isolation wideband mimo antenna for mm-wave applications, Electronics (switzerland) 10 (11) (2021) 1300, https://doi.org/10.3390/electronics10111300.
[17] Z. Cheng, M. Chen, H. Liu, M. Xia, W. Gong, Channel modeling for diffusion-based molecular MIMO communications using deep learning, Nano Commun Netw 42 (2024) 100543, https://doi.org/10.1016/j.nancom.2024.100543.
[18] K.R. Mahmoud, A.M. Montaser, Synthesis of multi-polarised upside conical frustum array antenna for 5G mm-Wave base station at 28/38 GHz, IET Microwaves Antennas Propag. 12 (9) (2018) 1559–1569, https://doi.org/10.1049/iet-map.2017.1138.
[19] D.T.T. Tu, N.T.B. Phuong, P.D. Son, V. Van Yem, Improving characteristics of 28/38GHz MIMO antenna for 5G applications by using double-side EBG structure, Journal of Communications 14 (1) (2019) 1–8, https://doi.org/10.12720/jcm.14.1.1-8.
[20] B. Aghoutane, S. Das, M. EL Ghzaoui, B.T.P. Madhav, H. El Faylali, A novel dual band high gain 4-port millimeter wave MIMO antenna array for 28/37 GHz 5G applications, AEU-Int. J. Electron. C. 145 (2022) 154071, https://doi.org/10.1016/j.aeue.2021.154071.
[21] W. Ali, S. Das, H. Medkour, S. Lakrit, Planar dual-band 27/39 GHz millimeter-wave MIMO antenna for 5G applications, Microsyst. Technol. 27 (2021) 283–292, https://doi.org/10.1007/s00542-020-04951-1.
[22] A. Ahmad, D. you Choi, S. Ullah, A compact two elements MIMO antenna for 5G communication, Sci Rep 12(1) (2022) 3608, doi: 10.1038/s41598-022-07579-5.
[23] D. Khan, A. Ahmad, D.Y. Choi, Dual-band 5G MIMO antenna with enhanced coupling reduction using metamaterials, Sci. Rep. 14 (1) (2024) 96, https://doi.org/10.1038/s41598-023-50446-0.
[24] S. Yue, S. Zeng, L. Liu, Y.C. Eldar, B. Di, Hybrid Near-Far Field Channel Estimation for Holographic MIMO Communications, IEEE Trans. Wirel. Commun. 23 (11) (2024) 15798–15813, https://doi.org/10.1109/TWC.2024.3433491.
[25] P.S. Manage, Dr.U. Naik, V. Rayar, Compact design of MIMO antenna with split ring resonators for UWB applications, Nano Commun Netw 41 (2024) 100512, doi: 10.1016/j.nancom.2024.100512.
[26] K. Pandya, T. Upadhyaya, U. Patel, V. Sorathiya, A. Pandya, A.J.A. Al-Gburi, M. M. Ismail, Performance analysis of quad-port UWB MIMO antenna system for Sub-6 GHz 5G, WLAN and X Band Communications, Results in Engineering 22 (2024) 102318, https://doi.org/10.1016/j.rineng.2024.102318.
[27] L. Zhang, H. Kou, Y. Pang, L. Yang, X. Zhang, Z. Shang, L. Zhang, Design of Temperature-Pressure Sensor Based on Slot-Antenna CSRR Integrated for applications in High-Temperature Environments, IEEE Sens. J. 24 (2024) 27218–27224, https://doi.org/10.1109/JSEN.2024.3423023.
[28] S. Islam, M. Zada, H. Yoo, Low-Pass Filter based Integrated 5G Smartphone Antenna for Sub-6-GHz and mm-Wave Bands, IEEE Trans. Antennas Propag. 69 (9) (2021) 5424–5436, https://doi.org/10.1109/TAP.2021.3061012.
[29] A. Kazmi, M. Zada, S. Islam, H. Yoo, Dual-Band MIMO Prototype in the Sub-6 GHz Integrated with mm-Wave Arrays: Ensuring Beamforming and Safety measures, IEEE Access 12 (2024) 38957–38971, https://doi.org/10.1109/ACCESS.2024.3374896.
[30] A. Sufyan, S.A.A. Shah, K.B. Khan, I.A. Shah, A. Ullah, T.A. Siddiquu, S. Islam, H. Yoo, Self-Decoupled 8-Element dual Polarized MIMO Antenna for B5G Handsets with Sub-6 GHz and mmWave Integration, IEEE Access 12 (2024) 167324–167332.
[31] M.K. Shereen, M.I. Khattak, A. Basit, G. Ahmad, Intelligent Frequency, Radiation Pattern and Polarization Reconfigurable Antenna for 5G applications, J. Electr. Eng. Technol. 19 (2024) 3339–3353, https://doi.org/10.1007/s42835-023-01718-2.
[32] T.A. Balarajuswamy, R. Nakkeeran, Reconfigurable SIW antenna at 28/38 GHz for 5G applications, Int. J. Interact. Des. Manuf. 17 (2023) 2977–2986, https://doi.org/10.1007/s12008-022-01143-1.